



Effect of (5%) CO₂ on the Oxidation Rate During Cooling of Industrial Aluminum White Dross

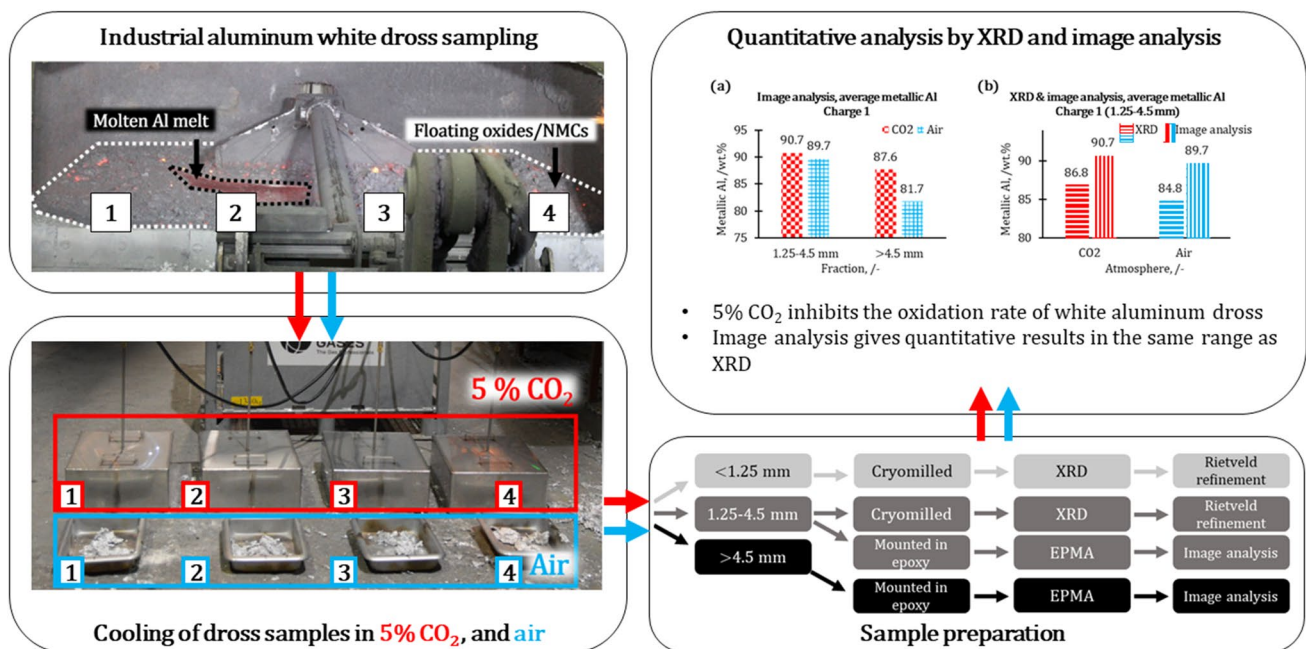
Cathrine Kyung Won Solem^{1,2} · Stefano Deledda³ · Hannes Zedel¹ · Gabriella Tranelli¹ · Ragnhild E. Aune¹

Received: 10 February 2023 / Accepted: 22 May 2023
© The Author(s) 2023

Abstract

Aluminum (Al) white dross is classified as hazardous waste and originates from the primary production of Al as a result of molten metal oxidation at an industrial scale. As the produced dross reduces the annual metallic Al production by up to 10%, finding a way to reduce the dross formation has always been of interest. Several laboratory studies have shown that exposing molten Al to small amounts of CO₂ has an inhibiting effect on the oxidation rate of the metal. Still, few studies have described this effect at an industrial scale. The present work has therefore studied the impact of protective cooling of industrial white dross samples on the oxidation rate of the dross to shed some light on the issue. Samples were collected from the holding furnace in a casthouse during the production of two different charges of Al alloys with varying amounts of magnesium (Mg), i.e., Charge 1 (AlMg1.0Mn0.4) and Charge 2 (AlMg1.2Mn0.4). The samples were cooled in ambient air and under a lid with 5% CO₂ mixed with 95% synthetic air in two parallels and later characterized by X-Ray Diffraction and Electron Probe MicroAnalysis combined with deterministic image analysis. Both methods confirm that all samples cooled under the protective atmosphere with 5% CO₂ had a higher content of metallic Al (89.4 wt%) than those cooled in ambient air (86.0 wt%), indicating that small amounts of CO₂ also inhibit the oxidation rate of dross at an industrial scale.

Graphical Abstract



The contributing editor for this article was Hojong Kim.

Extended author information available on the last page of the article

Keywords Aluminum · White dross · Oxidation · Inhibition of oxidation · Industrial sampling · Image analysis

Introduction

Oxidation of aluminum (Al) and its alloys results in dross formation during industrial Al production, causing losses of up to 10% of the annual Al produced [1]. The rate of oxidation of Al has proven to be influenced by several parameters that can have both amplifying or inhibiting effects, i.e., the magnesium (Mg) content which has proven to have amplifying effects, and inert atmospheres to be inhibiting [2–5].

During primary production of Al, white dross is the oxidation product with a metallic Al content varying from 40 wt% up to > 80 wt% due to different furnace processes [6–8]. The white dross is, in other words, highly heterogeneous, and it is also classified as a toxic and hazardous waste that should be managed in compliance with the current legislation. Landfilling of Al dross is forbidden in most European countries, and it must therefore be recycled and processed in a way that considers the environmental impact of the processing steps taken [9].

The Mg concentration in the Al alloy is reported to have a prompting effect on the dross formation resulting in an increasing oxidation rate [3, 10]. This effect is seen during production when adding Mg to the casthouse holding furnace, as well as at laboratory-scale experiments. As a result, higher Mg concentrations contribute to formation of MgO and MgAl₂O₄ and consequently breakaway oxidation [11].

Furnace operations also have an effect on the oxidation rate of Al. Before casting the Al alloy, it is necessary to stir the melt to assure complete dissolution of the solid alloying elements added [12]. This task is mainly carried out by one of the furnace operators using a large rake that is carefully stirred through the melt, see Fig. 1 [8]. The negative aspect of this step is that it disturbs and breaks up the oxide layers already formed and floating on top of the melt together with non-metallic compounds (NMCs) (areas marked with dotted

white lines in Fig. 1), and new unreacted molten surfaces are exposed to the surrounding atmosphere (area marked with a dotted black line in Fig. 1). New oxide films and layers are, as a result, formed allowing even more of the molten Al to oxidize and thereby influence the overall metallic yield [13].

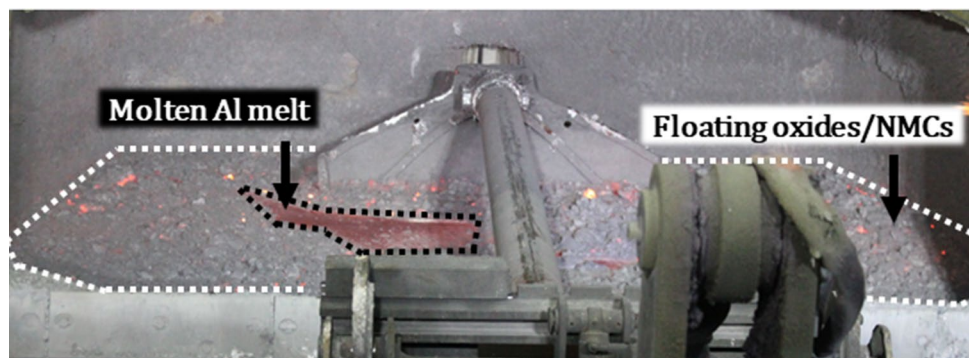
As previously described, adding certain elements, e.g., beryllium (Be) and calcium (Ca), to the melt can inhibit the oxidation rate of Al [5, 14, 15]. There are, however, some risks related to adding these elements, as Be is known to be harmful to humans [16], and Ca may cause cracking of the alloy when being further processed through rolling and forming operations of the final product [17].

Another inhibiting parameter is adding small amounts of CO₂ to the atmosphere/cover gas in contact with the molten alloy. Smith et al. reported an inhibiting effect adding from 50% down to 5% CO₂ to an atmosphere of synthetic air [18]. Further investigations using X-ray Photoelectron Spectroscopy (XPS) revealed a carbon (C)-containing oxide layer, concluded to form by reactions with the CO₂ in the atmosphere [19].

The present authors (Solem et al. [20]) also investigated the influence of adding small amounts of CO₂ (4%) to an oxidizing atmosphere and its effect during heat treatment of Al alloys 5182 (AlMg4.5Mn0.4) and 6016 (AlSi1.2Mg0.4). The results revealed that small amounts of CO₂ significantly reduced the mass gain for both alloys and influenced the oxide layer morphologies compared to when heat treated in synthetic air. It was also observed that the CO₂ adsorbed onto a nanocrystalline MgO surface and formed an amorphous C layer preventing further oxidation of Mg to MgO and MgO to MgAl₂O₄ [11, 20].

The inhibiting effect caused by CO₂ has only been studied at laboratory scale and not at an industrial scale in view of its effect on dross formation. To do so, a tool for systematically collecting representative dross samples

Fig. 1 Image of an aluminum (Al) melt being skimmed, where the oxides/non-metallic compounds (NMCs) are floating on top of the melt (marked with white). A small, cleaned area of the molten Al melt is also marked with a black dashed line



directly from the casthouse holding furnace was developed [21] and further modified by the present authors (Solem et al. [22]), supported by step-by-step procedures for sample collection, preparation, and analyses for quantifying the content of metallic Al, oxides, and other NMCs in the heterogeneous dross mixture collected. The developed tool was tested at an industrial campaign at Alcoa ANS in Mosjøen (Alcoa), Norway, and revealed to be well suited for collecting representative dross samples. The chosen sample preparation method (cryomilling) and analysis technique (X-ray diffraction (XRD)) proved to give reproducible results.

Based on the above, the present work aimed to investigate the effect of protective cooling of dross samples collected from the holding furnace at the casthouse facilities of Alcoa during the production of AlMgMn alloys with varying amounts of Mg. A cooling atmosphere of 5% CO₂ mixed with 95% synthetic air was used and compared to cooling performed in ambient air. XRD and Electron Probe MicroAnalysis (EPMA) combined with deterministic image analysis were used to analyze the results.

Experimental Set-Up and Procedure

The sampling tool and procedure for collecting representative industrial Al dross samples developed by Solem et al. [22] were applied in the present work. To enable protective cooling of the collected dross samples, lids were designed to cover the dross trays, which also allowed for a gas or gas mixture to be purged onto the dross while it was being cooled. It was also crucial that the set-up did not disturb normal furnace operations while, at the same time, minimizing air exposure during sample handling.

Design of Lids

The lids were made of stainless steel plates with a thickness of 2 mm. The shape chosen was rectangular with the dimensions 37 × 47 cm and a height of 16 cm, allowing one lid to cover one dross tray. A 43 cm long stainless steel pipe was welded to the top surface of the lid to allow gas to be purged onto the dross tray (gas inlet). The pipe's location was chosen so that the gas was distributed evenly over the full dimensions of the tray. Two holes on each short side of the lid were added to create an escape route for the gas (gas outlet). In addition, two handles were placed on the top of the lid to ease the lid's handling when placed over the dross tray or removed. The individual lids were connected by standard gas tubing to the gas bottles placed next to the holding furnace (Fig. 2).

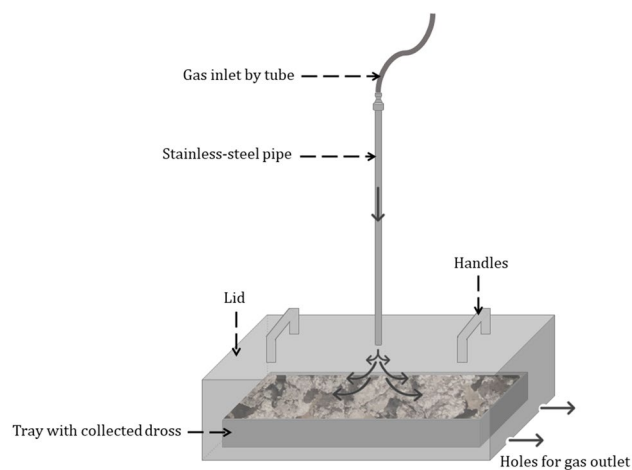


Fig. 2 Illustration of the lid and its use with the gas inlet on top and gas outlet on each short side

Sampling

The sampling tool designed and its use to secure reproducible dross samples from the casthouse holding furnace during one-furnace practice have been discussed elsewhere (Solem et al. [22]). In the present study, the tool was used to collect dross samples from two different AlMgMn charges during production, i.e., Charge 1 (AlMg1.0Mn0.4) and Charge 2 (AlMg1.2Mn0.4), where Charge 1 was collected at 772 °C, Charge 2 at 771 °C, and both charges were collected before fluxing (removal of alkali elements by purging chlorine or argon gas through the melt before casting) of the melt. It was, however, made one significant adjustment to the previously developed procedure and that was collecting two samples from each location instead of one.

The first dross sample that was collected was transferred to a dross tray and cooled in ambient air simulating the casthouse dross cooling conditions as there is currently no in-house dross press or Ar cooling procedures on site. The second sample was transferred to a tray and immediately placed under a lid to be cooled in a protective atmosphere of 5% CO₂ mixed with 95% synthetic air. The same sampling procedure was followed for all locations where samples were collected, i.e., Location 1 (closest to the injection point of primary produced Al), Location 2 (left of the center of the holding furnace), Location 3 (right of the center of the holding furnace), and Location 4 (furthest away from the injection point of primary produced Al). This resulted in two parallels of collected samples for each charge.

An image of the complete set-up is seen in Fig. 3, where the gas is connected to each lid, covering a dross tray for protective cooling (marked with a red box). The other sample collected from the same location was placed in front and cooled in ambient air (marked with a blue box).

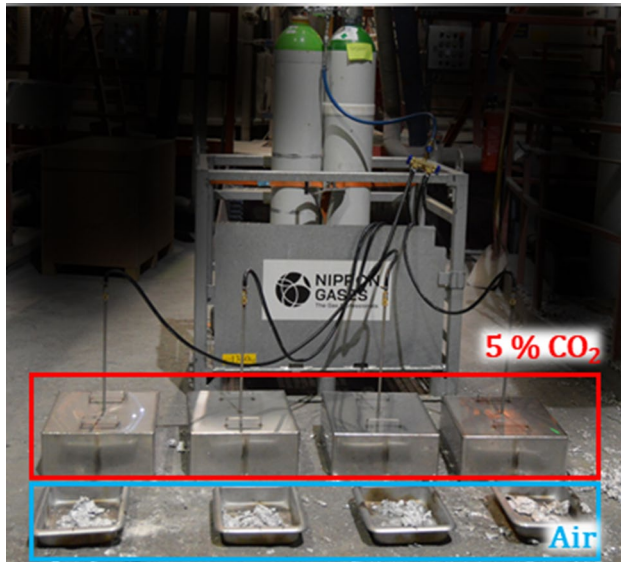


Fig. 3 Set-up for protective cooling of collected Al dross samples. Parallel samples are cooled under lids with a purging gas of 5% CO₂ mixed with 95% synthetic air (marked with red) and in ambient air (marked with blue)

To compare each sampled charge, the same person was responsible for collecting all the dross samples from the different locations in the holding furnace.

Figure 4 presents a flowchart showing the different steps that each dross sample collected from Charge 1 went through after being cooled, i.e., sieved into different fractions, pulverized, and characterized. Figure 5 shows the same for Charge 2.

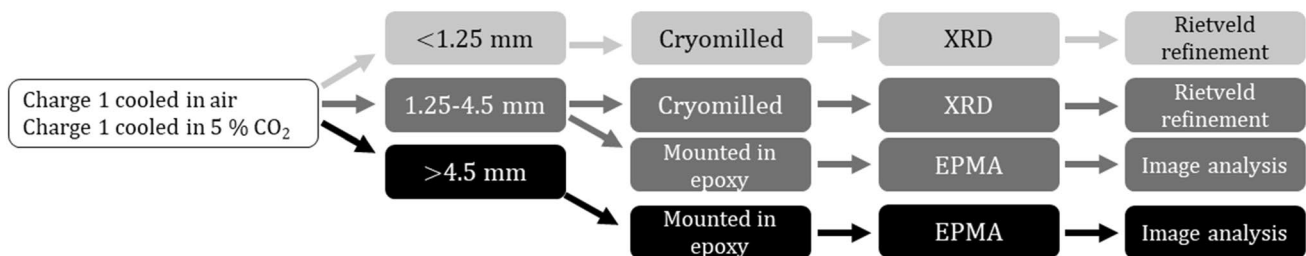


Fig. 4 Flowchart of the sample preparations and analysis for Charge 1

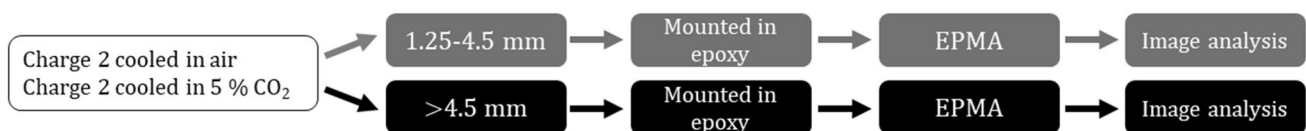


Fig. 5 Flowchart of the sample preparations and analyses for Charge 2

Sample Preparation

The two parallels of dross samples collected from each charge were sieved separately into three size fractions, i.e., < 1.25 mm, 1.25–4.5 mm, and > 4.5 mm. The smallest (< 1.25 mm) and mid (1.25–4.5 mm)-size fractions were pulverized by using cryomilling and later analyzed. Selected pieces of dross from the mid (1.25–4.5 mm)- and largest (> 4.5 mm) size fractions were mounted in epoxy and later analyzed.

Cryomilling of the Smallest and Mid-Size Fractions of the Dross Samples

A cryomilling unit from SPEX (6770 Freezer/Mill, USA) was used for crushing each dross sample. The unit consisted of a vial made of polycarbonate, a cylindrical impactor, and end pieces made of steel. To cool the samples down to $-196\text{ }^{\circ}\text{C}$ both before and during milling, liquid nitrogen (N₂) was used.

Each milling cycle consisted of a precooling step of 60 min to cool down the milling media and the samples, followed by 6 min of effective cryomilling and 3 min of pauses between the sequences. After three milling sequences, the apparatus was paused for the bath to be re-filled with liquid N₂ before the following milling sequence was started. This continued until an overall cryomilling time of 60 min was reached, which previously was reported by Solem et al. [22] to be sufficient for pulverizing the metallic Al lumps and flakes present as larger fractions in the dross. After finalizing the cryomilling, each sample was again sieved, and the portion of the sample that was < 100 μm was put aside for XRD analysis.

Mounting and Polishing of the Mid- and Large-Size Fractions of the Dross Samples

Eight randomly selected pieces of the dross from Charge 1 and Charge 2 were mounted in epoxy, polished with 1 μm diamonds, and dried in a cabinet at 65 $^{\circ}\text{C}$ for a minimum of 24 h before being coated with a 10–20 nm thin layer of C.

Quantitative Analyses

All collected dross samples that were cryomilled were analyzed by XRD, and all mounted samples were analyzed by EPMA combined with deterministic image analysis (described below). This allowed for comparing the obtained results and, thereby, reaching a higher degree of accuracy when interpreting the results.

X-Ray Diffraction

A D8 A25 DaVinci X-Ray Diffractometer (Bruker, Billerica, Ma, USA), equipped with a LynxEye™ superspeed detector and monochromatic $\text{CuK}\alpha$ photons with a wavelength of $\lambda = 1.5406 \text{ \AA}$, was used for the XRD analyses. A scattering angle of 2θ covering a range of 6–110 $^{\circ}$ was set, and an X-ray generator of 40.0 kV was applied for all measurements. Each XRD scan was carried out with a step size of 0.020 $^{\circ}$ and a step duration of 8 s/step with a fixed divergence slit of 0.100 $^{\circ}$. Rietveld refinement was performed for all scans using the TOPAS software (version 5, Bruker, Billerica, Ma, USA) to refine the data and quantify the phases present in each sample.

EPMA

A JEOL JXA-6500F Field Emission Electron Probe Micro-analyzer (JEOL Ltd., Tokyo, Japan) was used for the EPMA. The same set-up of the instrument was used for all samples, i.e., the same detector was used for each specific element to assure consistency in the element mapped, as well as the same magnification to allow for direct comparison of the microstructure and size.

Deterministic Image Analysis

For quantifying the elemental mappings in the EPMA scans, a previously established deterministic image analysis method was applied to 2D images where each pixel's intensity value represents the target element's concentration at its location [23]. As the deterministic image analysis results have been found to correlate well with the XRD results, e.g., having correlation factors of 0.924 and 0.916 (on a scale from 0 to 1, where 1 equals complete correlation) for the metallic Al phase and the oxides/NMCs phases, respectively, the

two quantitative analysis methods have been compared in the present work as well [23]. Multiple quantitative metrics were derived for detecting the targeted phases using deterministic image analysis. Each pixel was classified into one of the targeted phases by its predominant content, and by applying an intensity threshold to the elemental C, the map provided detection of pores and epoxy. Where no pores or epoxy were detected, an oxygen (O) threshold was used to determine the areas with a higher concentration of O representing non-metallics and areas with a lower concentration of O representing metallics. At a maximum, there were eight scans per experimental condition, of which one to two were discarded due to excessive cryolite content.

Each sample was distinctly divided into three different areas, i.e., (i) pores/epoxy-dominant areas, (ii) metallic areas, and (iii) non-metallic areas on a pixel-by-pixel basis, from the intensity thresholding of the elemental maps. The same thresholding was applied systematically for all EPMA scans to enable statistical pooling, comparisons, and the identification of trends. Based on this analysis, the relative content of each of the three phases per scan as a percentage of the total scanned area was determined. Each scan's relative metallic and non-metallic content was then pooled based on the experimental conditions for deriving means and medians per condition. An example is given in Fig. 6, where the EPMA results of Al (Fig. 6a), O (Fig. 6b), and C (Fig. 6c) are presented together with the CP image (the backscattered electron microscopy image) (Fig. 6d), as well as the phase detection based on the listed criteria above (Fig. 6e).

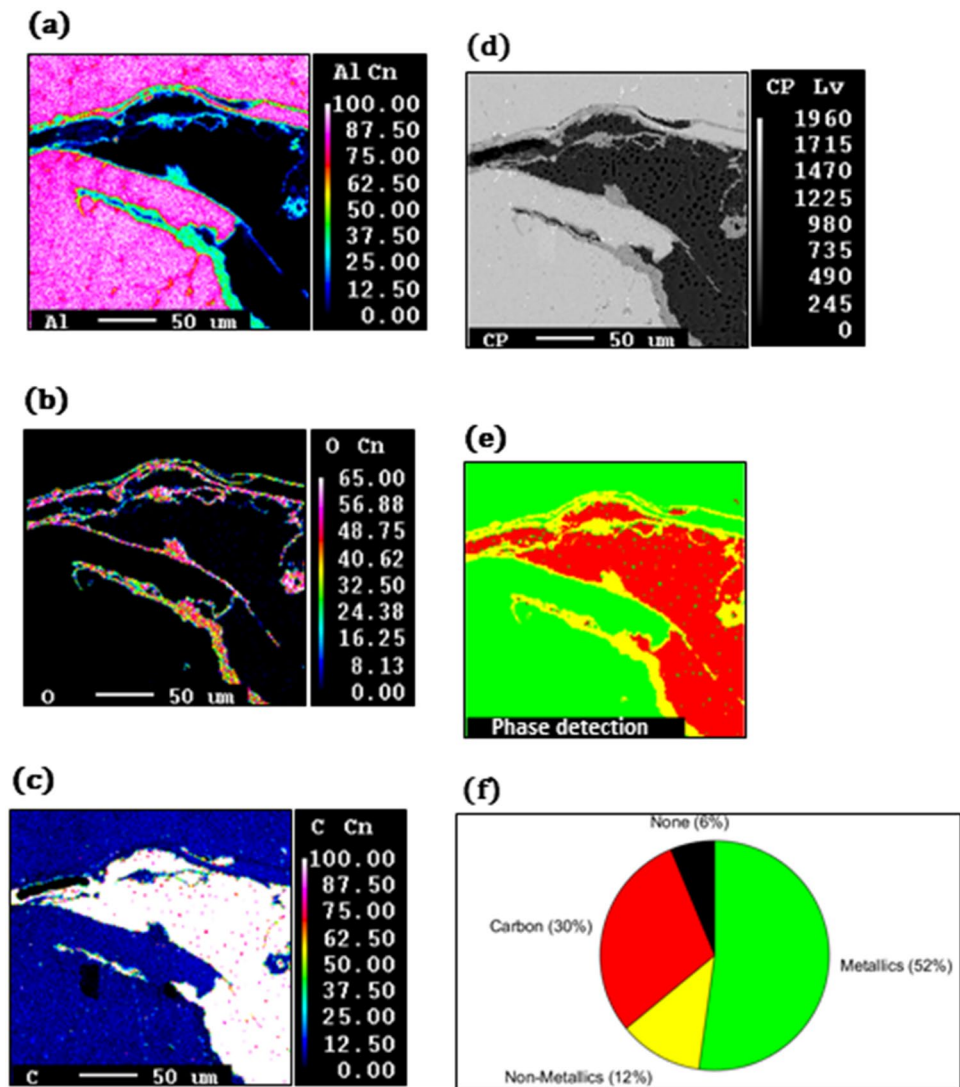
Results and Discussion

The effect of small amounts of CO_2 added to the atmosphere during protective cooling of industrial dross samples was (after sample preparation) evaluated by XRD, as well as EPMA combined with deterministic image analysis. XRD was chosen as it is a technique that gives unambiguous results and deterministic image analysis as it is a new and innovative approach with the ability to confirm the XRD results. Its method can also evaluate the presence of trace amounts that may be undetected by the XRD readings.

X-Ray Diffraction

The metallic Al content from the XRD measurements for the smallest fraction (< 1.25 mm) and the mid-fraction (1.25–4.5 mm) for Charge 1 cooled in CO_2 (red graphs) and in ambient air (blue graphs) for Location 1 and Location 4 are presented in Fig. 7a and b. As can be seen from the graphs, the metallic Al content is higher when cooled in CO_2 than in air for both fractions. It can also be seen that the metallic Al content is higher for the 1.25–4.5 mm

Fig. 6 EPMA results of **a** Al, **b** O, **c** C, **d** CP (backscattered electron microscopy) image, and **e** the binary phase detection based on those elements. A quantitative analysis is presented in **(f)**



fraction than for the < 1.25 mm fraction. Representative XRD results for Charge 1, fraction < 1.25 mm, for Location 1 and Location 4 for the metallic Al (Fig. 7a) and oxides/NMCs (Fig. 7c) are presented Fig. 8, where the triangles represent the metallic Al phase, and the stars represent the oxides/NMCs phases.

The oxide content in the dross at respective locations for each of the fractions is given in Fig. 7c for the smallest fraction (< 1.25 mm) and in Fig. 7d for the mid-fraction (1.25–4.5 mm). From the XRD results, an increasing oxide/NMCs content with decreasing metallic Al content was established to exist from Location 1 to Location 4. This confirms the earlier observations made by the present authors [22].

The metallic Al concentrations in the dross were observed to be slightly higher than earlier reported values [22], which is believed to be linked to the applied milling technique (more homogenous samples), as well as the protective

cooling step. As previously mentioned, cryomilling was used for milling both sample fractions, but it was not the obvious choice of sample preparation technique from the start. Ring milling was first tested on the smallest fraction of the dross samples, but the technique did not successfully mill the dross down to the fine powder needed for accurate XRD analyses (large Al flakes were observed to exist in the pulverized material), resulting in an inhomogeneous powder. Based on this, cryomilling was used on both fractions of the dross samples, allowing the metallic Al content in the different fractions to be directly compared with a higher degree of accuracy. The potential inhibiting effect on oxidation from using protective cooling by purging gas with 5% CO₂ directly onto the dross samples while being covered by lids could then also be more accurately studied.

Based on the experimental approach, the mid-fractions (1.25–4.5 mm) for both charges investigated proved to have a higher metallic Al concentration when cooled under

Fig. 7 X-Ray diffraction (XRD) results of Charge 1 cooled in CO₂ (red, vertically lined) and ambient air (blue, horizontal lines) for the metallic Al content of **a** fraction <1.25 mm and **b** fraction 1.25–4.5, and for the oxide/non-metallic compounds (NMCs) contents of **c** fraction <1.25, and **d** fraction 1.25–4.5 mm

protective conditions. This indicates that the oxidation process had been inhibited and that the earlier laboratory-scale findings, i.e., where the oxidation rate of Al alloys containing Mg was inhibited when exposed to small amounts (4%) of CO₂ during cooling, had been reproduced through protective cooling under industrial conditions.

EPMA and Image Analysis

The EPMA results for two of the analyzed Al dross samples from Charge 1, i.e., fraction >4.5 mm from Location 1, are presented in Fig. 9. Their respective scanning electron microscopy (SEM) images are shown in the first row, where the sample in Fig. 9a is cooled under a lid with 5% CO₂ and b in ambient air. The EPMA results for the elements Al (second row), Mg (third row), and O (fourth row) are also presented in the same figure, where the left column is the sample cooled in 5% CO₂ and the right in ambient air.

As can be seen from the EPMA results, it is confirmed that the collected dross samples are strongly heterogeneous, as it varies from dense metallic Al areas with thin films and small MgO areas (left column) to highly oxidized areas consisting of larger areas of MgO/MgAl₂O₄ and Al₂O₃ (right column). The respective scale bars based on the experimental calibration are also given for each element.

It can also be seen from Fig. 7 that the samples protectively cooled under a lid with 5% CO₂ had, on average, a higher metallic Al content than the sample cooled in ambient air. However, it should be taken into account that the dross samples are highly heterogeneous. As a result, pure metallic Al areas are also recognized for some samples cooled in ambient air and highly oxidized areas for those cooled under a lid with 5% CO₂.

The average metallic Al contents identified by deterministic image analyses of the EPMA results for Charge 1 at Location 1 to Location 4 for the 1.25–4.5 mm and >4.5 mm fractions are presented in Fig. 10a, where the dross samples cooled under a protective atmosphere of 5% CO₂ are shown to the left (red checkered graphs) and in ambient air to the right (blue squared pattern). Even in this case, the figure shows that a higher metallic Al content is obtained for both fractions when cooled under a lid with 5% CO₂ than in ambient air, following the previously observed trends obtained at laboratory scale [11]. The results are, however, not consistent with the trend of having higher metallic Al content for larger fractions [24]. This deviation is believed to originate from the number of dross samples analyzed. In the present study, eight randomly selected

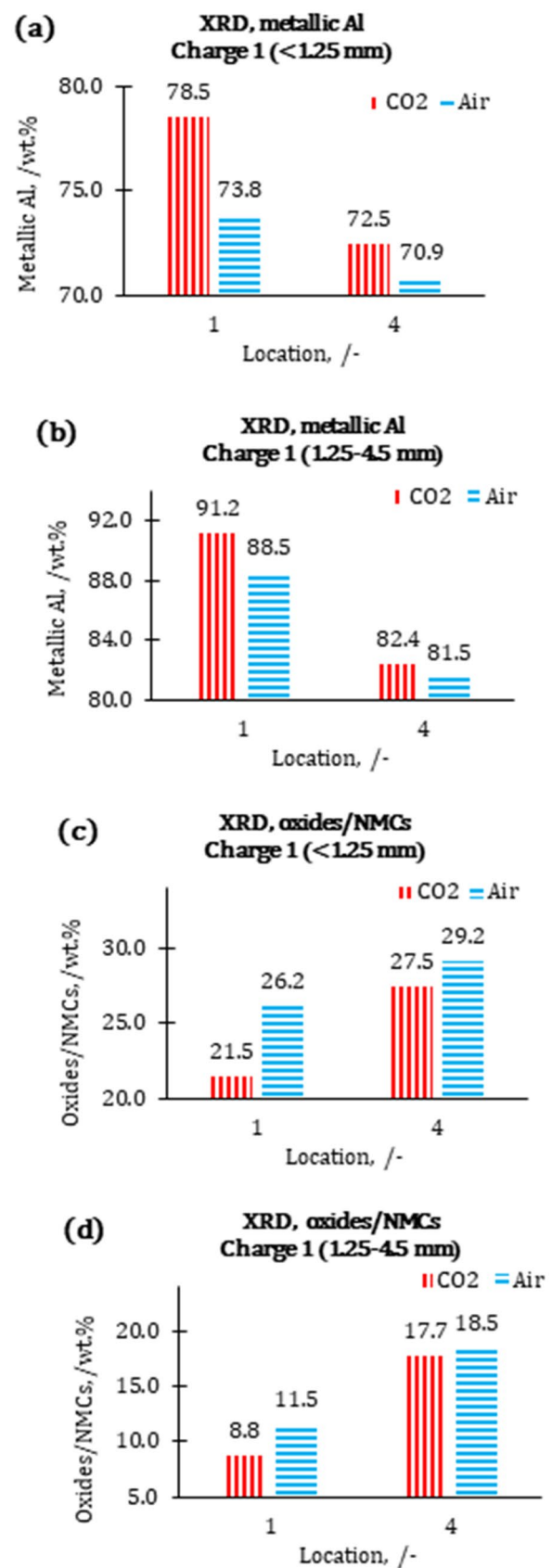


Fig. 8 XRD results of Charge 1, fraction <1.25 mm for **a** Location 1 cooled in CO₂, **b** Location 4 cooled in CO₂, **c** Location 1 cooled in air, and **d** Location 4 cooled in air, where the measured profile (black diamonds), fitted profile (light gray), and difference between measured and fitted profile (dark gray) profiles are presented. The Metallic Al phase is marked with triangles, and oxides/NMCs with stars

samples were considered for deterministic image analysis from each location, giving 32 samples for each fraction and for each cooling atmosphere (a total of 256 samples). In view of this, it should be noted that some samples were not included in the analysis as they proved to consist of pure cryolite. The overall result showed that the dross samples cooled under a protective atmosphere of 5% CO₂ had an average metallic Al content of 89.4 wt% when including both Charge 1 and Charge 2, as well as Location 1–4 for both fractions 1.25–4.5 and >4.5 mm, compared to 86.0 wt% metallic Al when cooled in ambient air.

When comparing XRD and deterministic image analysis results, see Fig. 10b, results in the same order of magnitude are obtained (striped graphs to the left represent the XRD results, and the squared graphs to the right the deterministic image analysis). Using XRD data as a reference, being an established method, validates the novel quantitative analysis of the EPMA scans as a possible approach for observing trends with similar metrics.

Summary and Conclusions

The present study investigated whether protective cooling of industrial Al white dross samples would influence the oxidation rate of Al. Two parallels of dross samples were collected directly from the casthouse holding furnace, of which one parallel was cooled under a lid purged with 5% CO₂ mixed with 95% synthetic air and the other in ambient air (casthouse atmosphere). The samples were further sieved, pulverized, and analyzed to determine their metallic Al content, as well as the oxide/NMC concentrations.

It is concluded that the CO₂-enriched atmosphere inhibits the oxidation rate of the industrial dross samples, confirming earlier observations from laboratory trials. From the XRD analysis, it is also established that the industrial dross samples cooled under a lid purged with 5% CO₂ have a higher metallic Al content for all fractions than for those cooled in ambient air. These results were further confirmed by EPMA combined with deterministic image analysis.

Future Work

Future work will continue to investigate the influence of different ratios of CO₂ on the oxidation rate of industrial white dross samples, at different temperatures. This will also include dross samples that have been processed by

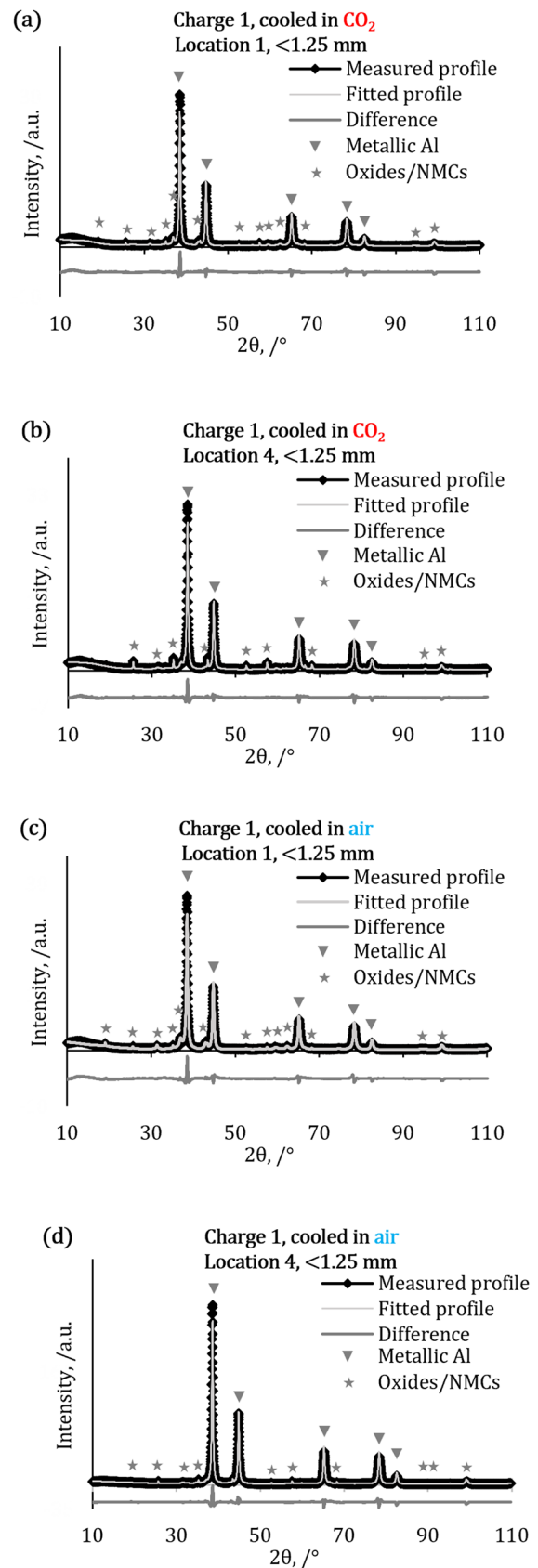
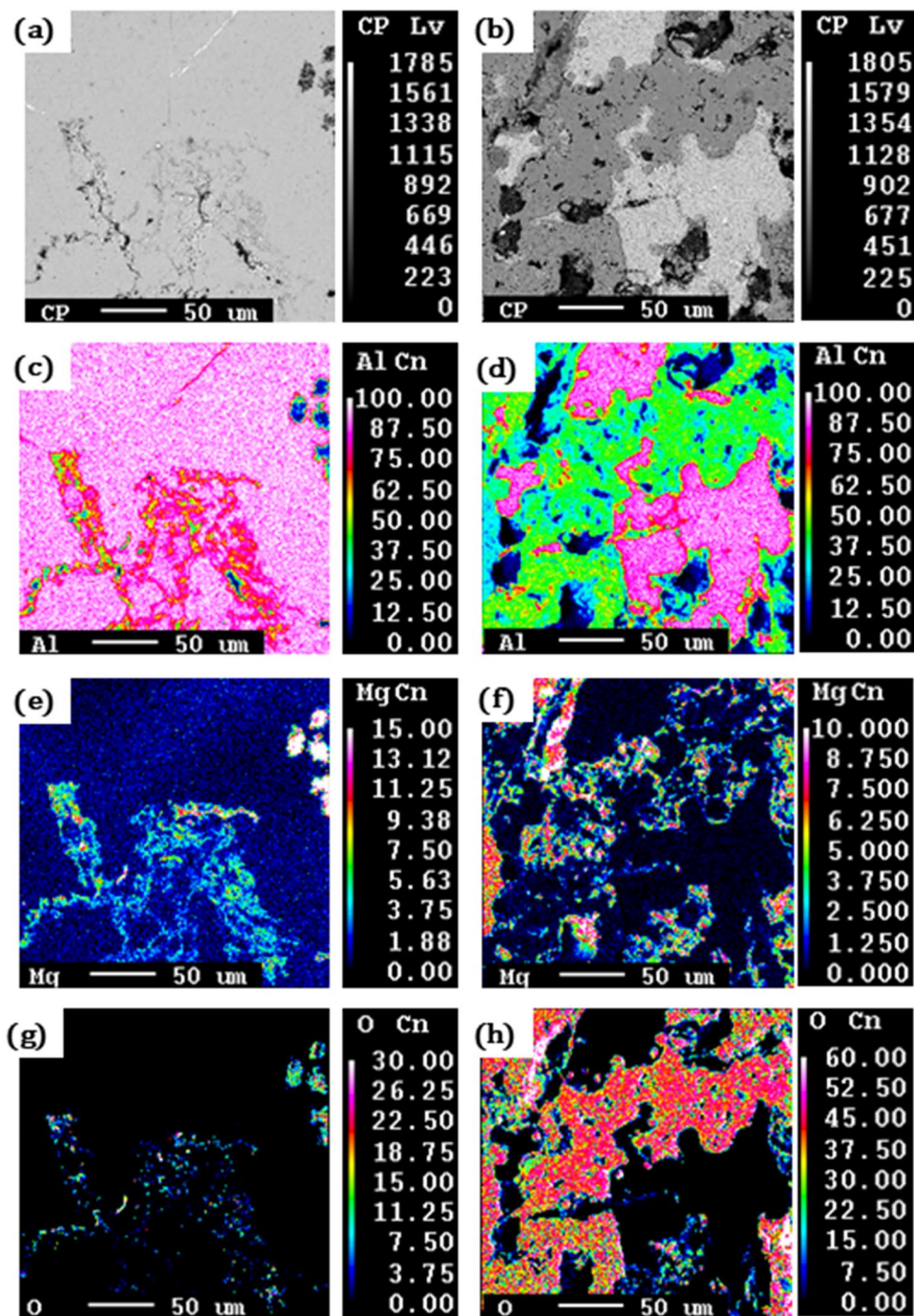


Fig. 9 Representative Electron Probe MicroAnalysis (EPMA) results of the collected dross samples for the elements Al (second row), Mg (third row), and O (fourth row), where the left column is dense Al areas with thin films, and the right column is a highly oxidized sample having larger areas with Al_2O_3 and $\text{MgO}/\text{MgAl}_2\text{O}_4$. Both samples are collected from Charge 1, Location 1, where the left sample has been cooled under a lid with 5% CO_2 and the sample to the right in ambient air



different in-house dross processing routes. Transmission electron microscopy (TEM) will also be carried out on such samples to see if an amorphous C layer is present

on the surface of the samples cooled under the protective atmosphere.

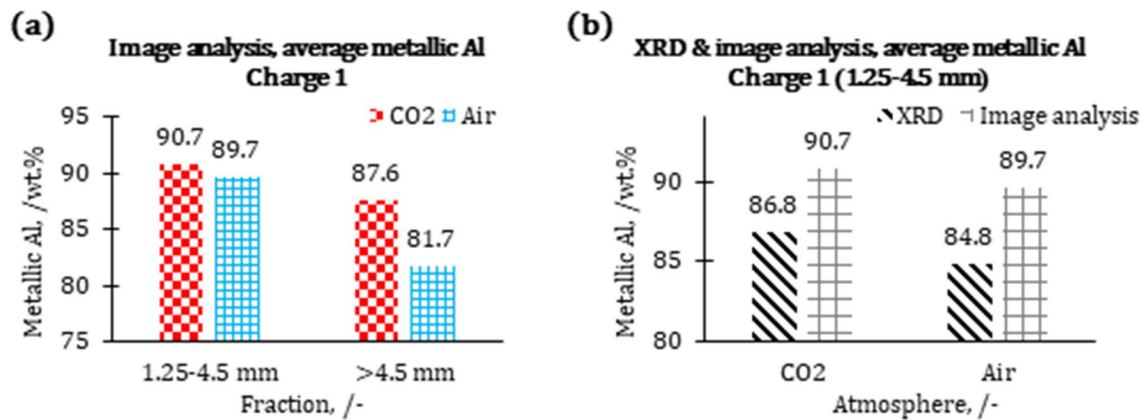


Fig. 10 Results from the deterministic image analysis showing the metallic Al content, i.e., **a** as a function of fraction comparing the samples cooled in 5% CO₂ (left graphs, red) and ambient air (right

graphs, blue), and **b** as a function of the atmosphere where the deterministic image analysis (checkered graphs) is compared with the XRD results (striped graphs)

Acknowledgements The authors gratefully acknowledge the financial support from the Research Council of Norway and the partners of SFI Metal Production. Special gratitude is given to Alcoa ANS for allowing us to collect the industrial dross samples from their site at Mosjøen, Norway, and to their operators for assisting during the industrial campaigns and sampling.

Funding Open access funding provided by NTNU Norwegian University of Science and Technology (incl St. Olavs Hospital - Trondheim University Hospital). This research has been funded by SFI Metal Production (Centre for Research-based Innovation, 237738).

Data Availability The data used to support the findings included in this publication can be accessed on request.

Declarations

Conflict of interest The authors declare that they have no conflict of interest.

Open Access This article is licensed under a Creative Commons Attribution 4.0 International License, which permits use, sharing, adaptation, distribution and reproduction in any medium or format, as long as you give appropriate credit to the original author(s) and the source, provide a link to the Creative Commons licence, and indicate if changes were made. The images or other third party material in this article are included in the article's Creative Commons licence, unless indicated otherwise in a credit line to the material. If material is not included in the article's Creative Commons licence and your intended use is not permitted by statutory regulation or exceeds the permitted use, you will need to obtain permission directly from the copyright holder. To view a copy of this licence, visit <http://creativecommons.org/licenses/by/4.0/>.


References

- Taylor JA, Prakash M, Pereira GG et al (2010) Predicting dross formation in aluminium melt transfer operations. In: Materials Science Forum. <https://www.scientific.net/MSF.630.37>. Accessed 2 Nov 2018
- Gomez A, Lima NB, Tenorio JAS (2008) Quantitative analysis of aluminum dross by the rietveld method. Mater Trans 49:728–732. <https://doi.org/10.2320/matertrans.MRA2007129>
- Cochran CN, Sleppy WC (1961) Oxidation of high-purity aluminum and 5052 aluminum-magnesium alloy at elevated temperatures. J Electrochem Soc 108:322–327. <https://doi.org/10.1149/1.2428080>
- Miresmaeili SM (2009) Effect of strontium on the oxidation behavior of liquid Al–7Si alloys. Oxid Met 71:107–123. <https://doi.org/10.1007/s11085-009-9136-3>
- Ha S-H, Yoon Y-O, Kim SK (2014) Effect of Al₂Ca on oxidation resistance and tensile property of Al–5Mg alloy. J Korea Foundry Soc 34:194–199. <https://doi.org/10.7777/jkfs.2014.34.6.194>
- Meshram A, Gautam D, Singh KK (2020) Recycling of white aluminium dross: production of potash alum. Trans Indian Inst Met 73:1239–1248. <https://doi.org/10.1007/s12666-020-01973-1>
- Abdulkadir A, Ajayi A, Hassan MI (2015) Evaluating the chemical composition and the molar heat capacities of a white aluminum dross. Energy Procedia 75:2099–2105. <https://doi.org/10.1016/j.egypro.2015.07.326>
- Peterson RD (2011) A Historical perspective on dross processing. Mater Sci Forum 693:13–23. <https://doi.org/10.4028/www.scientific.net/MSF.693.13>
- AlCircle. Aluminium dross processing: a global review. <https://www.alcircle.com/specialreport/306/drossprocessing>. Accessed 22 Oct 2020
- Bergsmark E, Simensen CJ, Kofstad P (1989) The oxidation of molten aluminum. Mater Sci Eng A 120–121:91–95. [https://doi.org/10.1016/0921-5093\(89\)90723-5](https://doi.org/10.1016/0921-5093(89)90723-5)
- Solem CKW, Vullum PE, Tranell G, Aune RE (2022) Heat treatment of Mg-containing aluminum alloys 5182 and 6016 in an oxidizing atmosphere with 4% CO₂. In: Eskin D (ed) Light metals 2022. Springer, Cham, pp 587–593
- Bui RT, Perron J (1988) Performance analysis of the aluminum casting furnace. Metall Mater Trans B 19:171–180. <https://doi.org/10.1007/BF02654201>
- Bonner SJ, Taylor JA, Yao J-Y, Rhamdhani MA (2016) Oxidation of commercial purity aluminum melts: an experimental study. In: Sadler BA (ed) Light metals 2013. Springer, Cham, pp 993–997

14. Glazoff MV, Rashkeev SN (2010) Beryllium adsorption at transition aluminas: implications for environmental science and oxidation of aluminum alloys. *J Phys Chem C* 114:14208–14212. <https://doi.org/10.1021/jp1044942>
15. Smith N, Gleeson B, Kvithyld A, Tranell G (2017) Effects of 2 ppm beryllium on the oxidation of a 5XXX aluminum alloy at temperatures between 500 and 750 °C. In: Ratvik AP (ed) *Light metals 2017*. Springer, Cham, pp 1465–1474
16. Cooper RG, Harrison AP (2009) The uses and adverse effects of beryllium on health. *Indian J Occup Environ Med* 13:65–76. <https://doi.org/10.4103/0019-5278.55122>
17. Yancey DD, DeYoung DH (1997) Calcium contamination of molten Al-Mg alloys by calcium carbonate. *Light Metals 1997*:1035–1041
18. Smith N, Gleeson B, Saidi W et al (2019) Effects of CO₂ cover gas and yttrium additions on the oxidation of AlMg alloys. In: Chesonis C (ed) *Light metals 2019*. Springer, Cham, pp 1025–1032
19. Smith N, Gleeson B, Saidi WA et al (2019) Mechanism behind the inhibiting effect of CO₂ on the oxidation of Al-Mg alloys. *Ind Eng Chem Res* 58:1434–1442. <https://doi.org/10.1021/acs.iecr.8b04691>
20. Solem CKW, Vullum PE, Ebadi M et al (2022) The role of CO₂ in the oxidation-protection of Mg-containing aluminum alloys. *Metall Mater Trans B*. <https://doi.org/10.1007/s11663-022-02524-3>
21. Kvithyld A, Bao S, Nordmark A et al (2014) Development of a sampling device for furnace dross. In: Grandfield J (ed) *Light metals 2014*. Springer, Cham, pp 931–935
22. Solem CKW, Deledda S, Tranell G, Aune RE (2022) Sampling procedure, characterization, and quantitative analyses of industrial aluminum white dross. *J Sustain Metall* 9:95–106
23. Solem CKW, Zedel H, Aune RE (2023) Characterization of low- and high Mg-containing aluminum white dross using deterministic image analysis of EPMA scans. In: Broek S (ed) *Light metals 2023*. Springer, Cham, pp 898–905
24. Kudyba A, Akhtar S, Johansen I, Safarian J (2021) Aluminum recovery from white aluminum dross by a mechanically activated phase separation and remelting process. *JOM* 73:2625–2634. <https://doi.org/10.1007/s11837-021-04730-x>

Publisher's Note Springer Nature remains neutral with regard to jurisdictional claims in published maps and institutional affiliations.

Authors and Affiliations

Cathrine Kyung Won Solem^{1,2}  · Stefano Deledda³ · Hannes Zedel¹ · Gabriella Tranell¹ · Ragnhild E. Aune¹

✉ Cathrine Kyung Won Solem
cathrine.k.w.solem@sintef.no

¹ Department of Materials Science and Engineering, Norwegian University of Science and Technology (NTNU), Alfred Getz Veg 2, 7034 Trondheim, Norway

² Department of Metal Production and Processing, SINTEF Industry, Strindvegen 4, 7034 Trondheim, Norway

³ Department for Hydrogen Technology, Institute for Energy Technology, 2027 Kjeller, Norway